APPLIED RESEARCH

Three-Phase Asynchronous Motor Fault Diagnosis Using Attention Mechanism and Hybrid CNN-MLP By Multi-Sensor Information

YI ZHOU[ID], QIANMING SHANG, AND CONG GUAN[ID], (Member, IEEE)
School of Naval Architecture, Ocean and Energy Power Engineering, Wuhan University of Technology, Wuhan 430063, China

Corresponding author: Qianming Shang (sqmte@whut.edu.cn)

ABSTRACT Single-signal-driven fault diagnosis has been widely applied in motor fault diagnosis, but it cannot meet the diagnostic requirements of complex motor systems. This study proposes a motor fault diagnosis method using attention mechanism (AM) and hybrid CNN-MLP by multi-sensor information. Firstly, Fast Fourier transform and continuous wavelet transform are performed on different signals to obtain the corresponding frequency domain feature information and wavelet time-frequency map images. A hybrid CNN-MLPAM model is used to extract features from spectral feature information and wavelet time-frequency images, respectively, and is trained to obtain preliminary classification results. Finally, a dynamic weight distribution vector is used to obtain the final diagnosis. The proposed method is verified by current, and vibration signals. The results show that the method can dynamically evaluate the sensitivity of different detection signals to different faults. The proposed method is more accurate and stable in fault diagnosis than the traditional method that relies solely on vibration signals. Under the consideration of time cost and diagnostic accuracy, the proposed CNN-MLPAM has higher diagnostic performance compared with CNN-RNNAM and CNN-ELMAM.

INDEX TERMS Fault diagnosis of motor, deep learning, attention mechanism, multi-sensor information.

I. INTRODUCTION

The electric motor is a complex device where various physical processes like mechanical, electrical, magnetic, thermal, etc., along with multiple unit technologies, are integrated into an electromechanical carrier to form the overall functionality. However, in recent years, the capacity and functions of motor systems have been expanded, and the load has increased, which has led to an increase in the probability of system failures with complex behavior patterns. For example, uneven mass distribution of the motor rotor can lead to rotor imbalance faults. Overloading or torque impact can cause rotor bending. Improper alignment during rotor installation or motor operation results in rotor eccentricity. These faults can lead to bearing wear, mechanical vibration, and increased noise in the motor. This reduction in service quality can even

lead to major catastrophic accidents, causing huge economic losses and adverse social impacts [1]. Therefore, fault diagnosis technology has become significant to complex motor systems.

The vibration, current, magnetic, and other signals can detect the motor fault. Different types of faults have different levels of sensitivity to different detection methods. For example, signals measured by the vibration method may be more accurate for mechanical faults [2], [3], while electrical faults diagnosed through current signals may have higher accuracy [4], [5]. Most of the traditional fault diagnosis methods are not carried out in relevant research.

The early description of motor fault states was the belief that symmetry related to the operation of the motor was damaged, resulting in abnormal effects on the operation of the motor, these phenomena include 1) unbalanced current and voltage signals; 2) mechanical vibrations and audible noise; 3) temperature changes; 4) irregular air gap magnetic flux

The associate editor coordinating the review of this manuscript and approving it for publication was Paolo Giangrande[ID].

changes; 5) instantaneous output power and torque changes; 6) speed changes. Early detection of these failures allows there placement of the motor component rather than replacing the complete motor [6]. However, the common cause of motor failure is bearing defects, rotor defects, insulation failure, and stator winding failures. The research progress of induction motor fault diagnosis using different measurement methods, such as current, voltage, vibration, temperature, sound, and electromagnetic signal analysis, is analyzed according to the available fault detection methods for different fault phenomena, as shown in Table 1. In [8], an approach to detect stator fault in adverse industrial conditions is presented, the approach uses extreme gradient boosting to evaluate temporal, spectral, and wavelet features of three-phase induction motor current signals, which provides an understanding of how each feature affects the diagnostic model over a wide range of voltage unbalances and torque values. In [9], this paper aims to detect a stator inter-turn short circuit in a synchronous machine through the analysis of the external magnetic field measured by external flux sensors. Long et al. [10] suggested a dynamic fusion AdaBoost classification method based on an attention mechanism, which improved the model's ability to collect key features and increased the motor fault diagnosis precision and robustness. Choudhary et al. [11] used multi-input convolutional neural network (MI-CNN) technology to fuse the characteristics of vibration signals and acoustic signals and proposed a vibration-acoustic fusion technology for the fault diagnosis of induction motors under different working conditions. This method can accurately and efficiently achieve the fault diagnosis of the motor and can be applied to other rotating machinery. In [12], this paper proposed an improved diagnosis method for early detection and localization of Inter-Turn Short Circuit (ITSC) faults in the stator winding of the induction motor (IM), which is achieved by using a novel indicator that is based on the Discrete Wavelet Energy Ratio (DWER) of three stator currents, with Artificial Neural Network (ANN). Xu et al. [13] proposed a global context residual network framework, which can fully mine the multi-scale information of the signal to realize motor fault identification under variable working conditions. Fu et al. [14] proposed a new multi-sensory fusion motor fault diagnosis model, named dynamic routing-based multimodal neural network (DRMNN), a dynamic routing algorithm is introduced in the decision layer of DRMNN to adaptively assign proper weights to different modalities. Glowacz [15] proposed a method of feature extraction of acoustic signals - SMOFS-22-MULTIEXPANDED (Shortened Method of Frequencies Selection Multi-expanded) was developed and implemented, and the nearest neighbor classifier is used to classify various fault types of motor. Xiao et al. [16] have utilized the variant of variational autoencoder (VAE) named deep mutual information maximization (DMIM) with variational divergence estimation approach to maximize the mutual information between input and output of the neural network to learn

representative features, which can generate new samples based on the representative features. Mohammed and Djurovic [17] proposed a stochastic monitoring scheme for the temperature of the stator windings in permanent magnet synchronous motors using end-winding-embedded circular fiber Bragg grating (FBG) thermal sensor arrays. Ullah et al. [18] investigated the unique variation trends of the torque angle in different fault conditions of permanent magnet synchronous motors. They proposed an inverter compensation technique based on the torque angle for online detection and identification of stator-to-rotor winding short-circuit faults and partially irreversible demagnetization faults. Ren et al. [19] proposed a fault diagnosis method based on motor speed and kurtosis spectral analysis, which can facilitate the extraction of impact components and improve the signal-to-noise ratio.

Although the methods for motor fault diagnosis are rapidly developing and improving, there are still inherent drawbacks. For example, some methods require sensors to be added to the motor to obtain signals such as vibration, magnetic field, acoustic, or current, which increases cost and complexity and may affect the normal operation of the motor. However, compared with magnetic signals, current signals have advantages such as easy collection, high accuracy, low noise, and convenient monitoring [4], [5]. Indeed, acoustic signals are prone to interference from environmental noise, this can make it challenging to effectively capture the target signal for acoustic fault diagnosis, particularly in noisy industrial environments where different types of machinery and equipment are operating simultaneously. In addition, some methods lack generality and are only applicable to specific types and specifications of motors, making it difficult to promote and apply them. Furthermore, some methods have high time and computational costs, requiring a large amount of computing resources and processing time, which also limits their application in real-time and online scenarios. Therefore, the design of efficient, reliable, and widely applicable methods for motor fault diagnosis is still a problem that needs to be deeply researched.

Numerous machine-learning tools have been utilized. For example, Hu et al., use Random Forests to determine fault types, based on extracted multi-scale dimensionless indicators as fault features [20]. Singh and Shaik combined Stockwell transform (ST) to extract the fault characteristics of motor stator current signals and feed these characteristics to different support vector machine (SVM) models for the detection of motor stator short circuits and ground faults [21]. Yaman proposed a multi-level feature generation approach that combines discrete wavelet transform with the local binary pattern (LBP) method to select the most informative features for the SVM and K-Nearest Neighbor (KNN) classification algorithms. The selected features are then used to determine the fault classification of induction motors [22].

Deep neural networks have demonstrated tremendous potential in mechanical fault diagnosis [23]. Li et al.

TABLE 1. Summary of ten papers in the past five years.

Ref.	Fault type	Type of Data or Information Used	Data Processing Methods or Work Delivered
Choudhary et al. [11] (2023)	Broken bar rotor Rotor bow Rotor unbalance Rotor misalignment Bearing defects	Vibration and Acoustic	Constant Q-Non-Stationary Gabor Transform
Vitor et al. [8] (2023)	Turn-to-turn short-circuit faults	Current	Fast Fourier transform and Discrete Wavelet transform
Xu et al. [13] (2022)	Broken bar rotor Rotor bow Rotor unbalance High impedance fault Bearing defects	Vibration	One-dimensional convolutional neural networks
Irhoumah et al. [9] (2021)	Turn-to-turn short-circuit faults	Stray flux	Statistical time-domain features and Katz's fractal dimension with Linear Discriminant Analysis supported by Feedforward Neural Network.
Long et al. [10] (2021)	broken rotor bar fault stator short winding fault bearing fault	Current, Magnetic, and Vibration	Hilbert transform and Fourier transform
Xiao et al. [16] (2021)	Rotor bow Rotor misalignment Rotor unbalance Broken bar rotor Bearing defects	Vibration	One-dimensional convolutional neural networks
Cherif et al. [12] (2020)	stator inter-turn faults	Current	Discrete Wavelet transform
Fu et al. [14] (2020)	Rotor bow Broken bar rotor Bearing defects	Vibration and Current	Hilbert transform
Sonje et al. [7] (2019)	Turn-to-turn short-circuit faults	Current	Park's vector modulus (PVM) and Discrete Wavelet transform
Adam et al. [15] (2019)	Turn-to-turn short-circuit faults broken rotor bar faulty ring of squirrel-cage faulty bearing	Acoustic	SMOFS-22-MULTIEXPANDED (Shortened Method of Frequencies Selection Multi-expanded)
Mohammed *et al* [17] (2019)	Turn-to-turn short-circuit faults	Temperature	-
Zia Ullah et al [18] (2020)	Turn-to-turn short-circuit faults irreversible demagnetization fault	Torque angle	-
Ren et al. [19] (2019)	Bearing defects	Speed	Kurtosis spectrum

proposed a method for detecting inter-turn short circuit faults in permanent magnet synchronous motors based on conditional generative adversarial networks and optimized sparse autoencoders. Experimental results demonstrate that the proposed fault diagnosis method has high diagnostic accuracy [24]. Liu et al. proposed a multi-scale kernel-based residual convolutional neural network for motor fault diagnosis. This method incorporates residual learning based on multi-dimensional information fusion and visual knowledge into multi-scale neural networks, avoiding performance degradation and constructing a deeper network [25]. However, the structure of deep learning algorithms is more complex than previous artificial intelligence algorithms, requiring more computing resources and higher hardware requirements.

Based on the previous research foundation, this article proposes an intelligent fault diagnosis method for three-phase asynchronous motors based on a hybrid input. In the proposed hybrid model, the first stage, CNN implements fault diagnosis from continuous wavelet transform (CWT) images. The second stage is a multilayer perceptron (MLP) for processing the spectrum of current signals. Therefore, the proposed model combines two neural network architectures, using different data types as inputs - numerical and image. As will be shown, the resulting model provides higher diagnostic accuracy than standalone CNN and MLP.
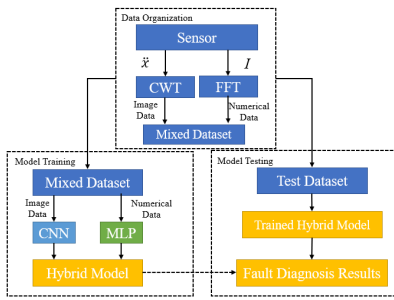
FIGURE 1. Overview of diagnostic methods.

The main contributions of this work can be summarized as follows:

1) A fault diagnosis method that simultaneously processes different types of data is proposed, which combines MLP for numerical inputs and CNN for CWT images, and a dynamic weight distribution vector is used to obtain the final diagnosis results with sub-classifiers.

2) Experiments on the dataset demonstrate that the proposed hybrid model is superior to CNN and MLP applied separately, and considering time cost and high diagnostic accuracy, CNN-MLPAM has higher cost-effectiveness compared to CNN-ELMAM, and CNN-RNNAM.

3) Comparing LSTM-BLS, VMD-CWT-CNN, PSO-CNN, and IGWO-DBN with CNN-MLPAM, it was found that solely utilizing motor vibration signals for motor fault diagnosis may limit the diagnostic performance of the models.

II. PROPOSED INTELLIGENT FAULT DIAGNOSIS METHOD

This section describes the hybrid fault diagnosis model that simultaneously processed data of different types. Figure 1 depicts an overview of the proposed method.

The implementation of the method is as follows.

Step 1: Convert signals from different sensors into mixed input data. The vibration signals are transformed into time-frequency images using CWT, which is suitable input for CNN. Similarly, three-phase current signals are converted into frequency spectrum by FFT, which is suitable inputs for MLP.

Step 2: Model training using the datasets specific to each model type, resulting in a well-trained hybrid model.

Step 3: Model testing. Use the trained hybrid model to identify bearing faults based on the mixed input data, with a sampling rate of 51.2 kHz.

A. CONVERT SENSOR SIGNALS INTO MIXED INPUT DATA

The three-phase AC asynchronous motor is operated at a constant speed of 1000r/min under a load of 50N∗m. Separated signals of vibration and three-phase current are measured by the vibration and current sensor. 256,000 data points(time-domain) are collected for both the current and vibratory signal for each fault motor.

TABLE 2. Similarity coefficients of different wavelet basis functions.

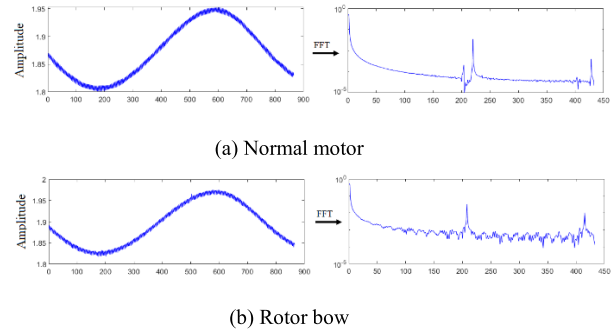| wavelet basis function	Morlet	Coif5	Db10	Meyer
similarity coefficient	7.2148	6.3298	7.4970	6.6082

(a) Normal motor

(b) Rotor bow

FIGURE 2. The a-phase current of motor FFT process.

As a common spectrum analysis method, FFT is widely used in motor fault diagnosis. The three-phase current signal is transformed to the frequency domain using FFT, and the sampling frequency is set at 48000 Hz. Different faults have different characteristic frequencies and rely on it to judge the type of fault of the motor. As shown in Figure 2, the frequency spectrum varies greatly from one motor state to another, and the three-phase current of the faulty motor has a dense and different harmonic component.

CWT is a time-frequency analysis method for non-smooth, non-linear signals. the motor vibration signal usually contains changes in time and frequency, so CWT can describe the characteristics of the motor vibration signal more comprehensively. CWT represents the signal through a family of wavelet functions. Le $\psi(t) \in L^2(R)$, which Fourier Transform is $\hat{\psi}(t)$, an $\hat{\psi}(0) = 0$, and the coefficient of the wavelet function ψ is the family of functions obtained by the telescopic translation:

$$\psi_{a,b}(t) = |a|^{-1/2} \psi\left(\frac{t-b}{a}\right) \quad (1)$$

where $\psi_{a,b}(t)$ a daughter wavelet function, defined as the mother wavelet ψ scaled in the frequency domain by a and translated in the time domain by b. $a, b \in \mathbb{R}$, and $a \neq 0$.

CWT features continuously scalable and translatable wavelets that allow a much more precise analysis of a signal's spectrum [7], as in

$$W_f(a,b) = |a|^{-1/2} \int f(t) \bar{\psi}\left(\frac{t-b}{a}\right) dt \quad (2)$$

where $\bar{\psi}$ corresponds to the conjugate of ψ.

When wavelet transform is applied to vibration signal and wavelet time-frequency map is drawn, the choice of wavelet basis function is directly related to the success of signal feature extraction, which affects the diagnosis result. However, wavelet basis functions are diverse and the choice usually involves a variety of properties, such as orthogonality, double
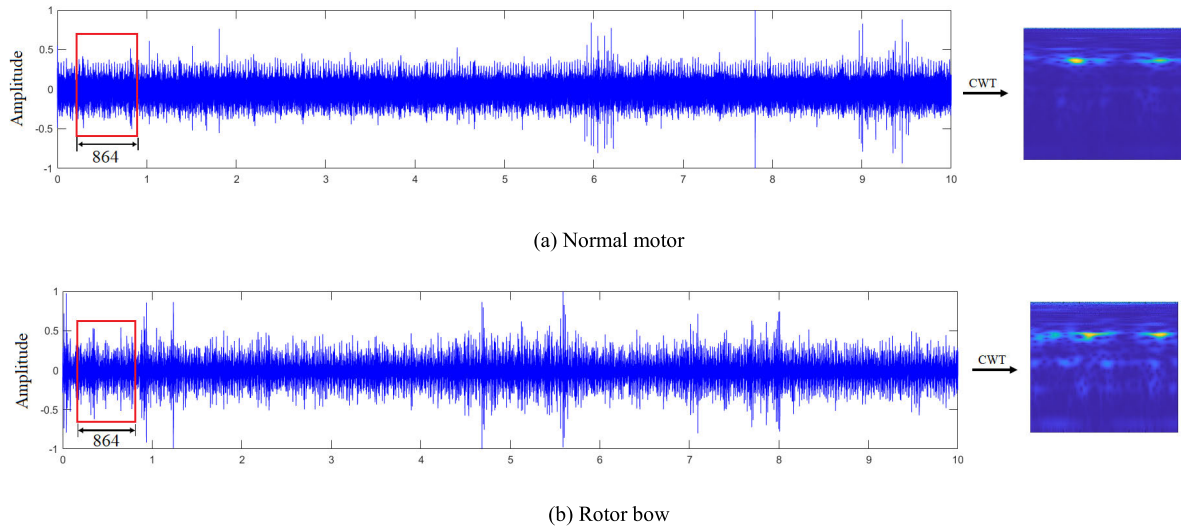
(a) Normal motor

(b) Rotor bow

FIGURE 3. Vibration signal of motor CWT process.
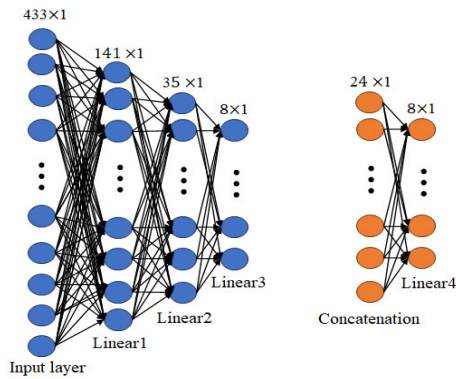

FIGURE 4. The network structures of MLP and FC.

orthogonality, tight support, symmetry, support length, and filter length of the function.

When the wavelet basis function is used to process other signals, the closer the waveform is to the shape of the impulse signal, the more signal features can be extracted [6]. The similarity between the wavelet basis function and the impulse signal can be expressed as in

$$\delta = \sum_{i=1}^{k} x_i \frac{m_i^2}{s_i} \tag{3}$$

where δ is the similarity coefficient, s_i is the area of each peak after taking the absolute value of the small wave base function, m_i is the maximum value of each peak after the absolute value of the small wave base function, k is the number of peaks obtained by taking the absolute value of the wavelet basis function.

The larger the similarity coefficient δ, the closer the waveform of the wavelet basis function is to that of the pulse signal. The similarity coefficients δ for four commonly used wavelet basis functions (Morlet, Coif5, Db10, and Meyer) are shown

in Table 2. The Db10 wavelet function is asymmetric, with poor smoothness and no explicit analytic equation.

Morlet wavelet basis function is a cosine signal with square exponential attenuation and explicit analytic equation. It has good symmetry and smoothness. Therefore, the Morlet wavelet basis function is more effective in extracting the fault feature information of a signal in wavelet transforms.

Figure 3 illustrates the process of transforming the vibration signals of a normal motor and a faulty motor into wavelet spectrograms. Data is processed as a series of overlapping windows, where each window has 864 data points. CWT is used to transform each vibration signal data window into a 64×64 time-frequency image to be processed by the CNN model. Simultaneously, FFT is applied to the corresponding three-phase current signal window to obtain the frequency spectrum. This process is repeated for subsequent overlapping data windows to produce the required data for training and testing.

B. ATTENTION MECHANISM CNN-MLP HYBRID MODEL

The attention mechanism CNN-MLP hybrid model mainly consists of three MLP branch modules, a CNN module, and an attention mechanism module, as shown in Figure 6. Specifically, the three MLP branch structures process the frequency spectra of the motor's phase currents a, b, and c, respectively, and extract numerical features under different motor conditions, the network structure of the MLP and fully connected (FC) layer is shown in Figure 4. The CNN primarily extracts high-dimensional features from wavelet spectrograms obtained under different motor conditions. The attention mechanism allocates reasonable weights to the training result vectors obtained from the two different measurement methods.

The inputs for the three MLP branches are obtained from the motor's three-phase current signals using the Fast Fourier
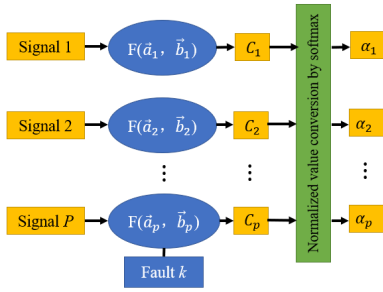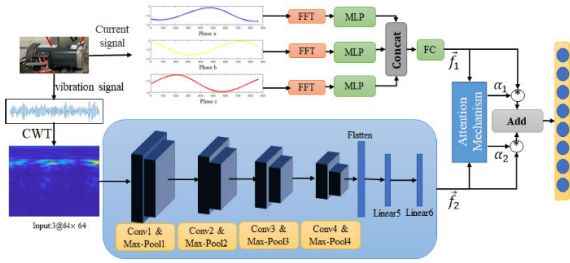
FIGURE 5. Flow chart of attention mechanism.

FIGURE 6. Hybrid CNN-MLPAM model with mixed input.

transform (FFT). The input for CNN is obtained from the vibration signals using the Continuous Wavelet Transform (CWT). The three MLP branches consist of multiple fully connected (FC) layers for feature learning and fusion of the three-phase current signals and employ an FC layer for dimensionality reduction. The CNN consists of multiple convolutional network units. The essence of the attention mechanism is weighted summation [4], The attention mechanism module assigns weights to the outputs of the three MLP branches and the CNN. Training result vectors $\vec{f}_i(i = 1, 2, \ldots, p)$ are obtained from P different measurement methods with different signals. The dimension of $\vec{f}_i$ is p.

$$f^* = \sum_{i=1}^{p} \alpha_i f_i \qquad (4)$$

In the proposed method of this paper, attention mechanisms rationalize the allocation of weights α_i, which generally involves two steps [10], as shown in Figure 5:

Step 1: Design a function F to calculates the score c_i^k of the ith measurement signal corresponding to the kth fault according to the P signals and q fault types. The score for each feature vector is based on the degree of correlation between signal f_i and the fault focused on by the attention mechanism. The greater corresponding score means the higher the correlation degree. As in

$$c_i^k = sim_i^k\left(\vec{f}_i, \vec{b}_i\right) = \frac{\vec{f}_i \cdot \vec{b}_i}{\left|\vec{f}_i\right| * \left|\vec{b}_i\right|} \qquad (5)$$

The cosine similarity [10] is used to distinguish the difference from the direction and space, and corrects the problem of inconsistent measurement standards between data, so it is adopted in this paper. Evaluate the similarity between the

TABLE 3. Description of the motor conditions.

Fault of Motor	Size of training/ testing samples	Label of condition
Normal	350/50	NM
Broken bar rotor	350/50	BR
Rotor misalignment	350/50	RM
Rotor bow	350/50	BW
Rotor unbalance	350/50	RI
Bearing defects	350/50	BF
Stator single-phase open	350/50	SP
Turn-to-turn short-circuit	350/50	SC

classification results $\vec{f}_i$ of different acquisition methods and the real results $\vec{b}_i$. The higher cosine similarity indicates that can reflect the more real situation of fault type.

Step 2: For the obtained scores $c_i^k(i = 1, 2, \ldots, p)$, the softmax function is constructed to get the corresponding weight. As in

$$\alpha_i = \text{softmax}(sim_i) = \frac{e^{sim_i}}{\sum_{j=1}^{p} e^{sim_j}} \qquad (6)$$

The outputs from the FC layer and CNN module are respectively taken as the classification result vectors of $\vec{f}_1$ and $\vec{f}_2$. The weights of the two outputs of α_1 and α_2 are calculated using the joint (4) and (5). Equation (3) is used to calculate the final classification result vectors of the FC layer and CNN module, which are added together.

III. EXPERIMENTAL ANALYSIS
A. DATASET INTRODUCTION
The experimental test bench used in this experiment is the Power Transmission Fault Diagnosis Comprehensive Test Bench designed by SpectraQuest. The test bench consists of a variable speed drive motor, a planetary gearbox, a parallel shaft gearbox supported by rolling bearings, a variable load magnetic brake, a set of vibration signal acquisition system, and a set of current signal acquisition system supported by rolling bearings, as shown in Figure 7. Sensor 1 is a vibration sensor, and its corresponding measurement result is Result 1. Sensor 2 is a current sensor, and its corresponding measurement result is Result 2. The variable speed drive motor used in this experiment is the Marathon_D396A asynchronous three-phase motor. In addition to a normal motor, the test bench is also equipped with a voltage unbalance fault motor, a phase loss fault motor, a turn-to-turn short-circuit fault motor, a rotor unbalance fault motor, and a rotor broken-bar fault motor for fault simulation.

The length of the current data and vibration data samples are set to 864 data points, and the vibration data is converted into a 64×64-sized wavelet time-frequency image. The three-phase current of the motor is also subjected to Fourier transform, and data of spectral length 433 is obtained. Each motor's operating state is sampled 500 times, resulting in a total of 4000 samples for the 8 motor operating states. This includes 4000 wavelet time-frequency images and
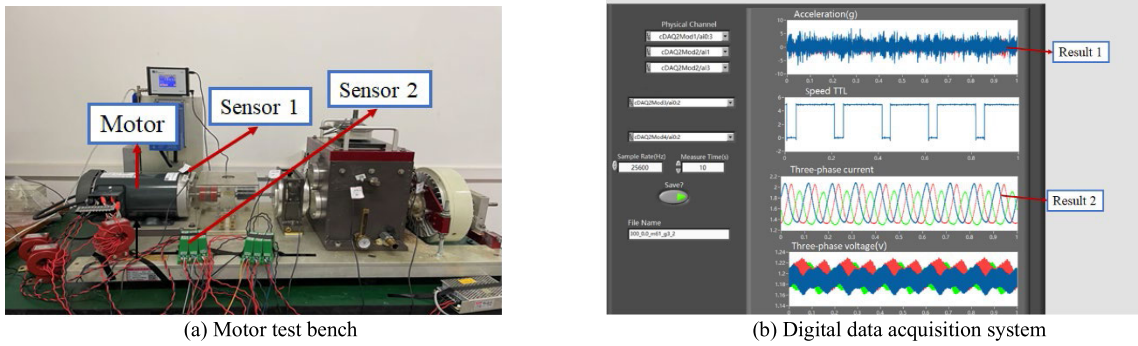
(a) Motor test bench

(b) Digital data acquisition system

FIGURE 7. Motor fault diagnosis platform.

(a)SP   (b)SC   (c)RM   (d)BR
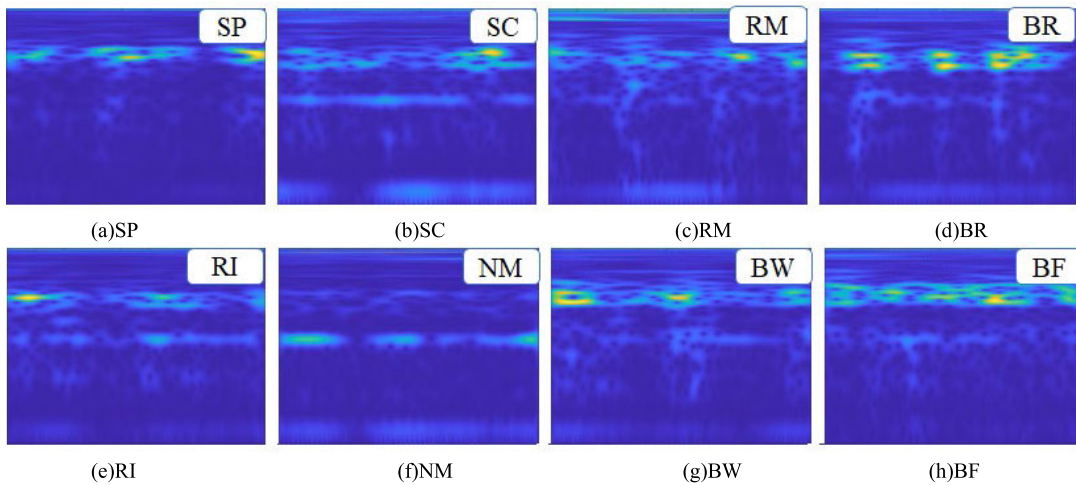
(e)RI   (f)NM   (g)BW   (h)BF

FIGURE 8. Wavelet time-frequency image of each motor state.

4000 motor three-phase current frequency spectrum samples. Finally, the samples are divided into training set, test set, and validation set in a 7:2:1 ratio, as shown in Table 3.

The wavelet time-frequency images of the motor in the 8 fault states are shown in Figure 8. The horizontal axis of the wavelet time-frequency images corresponds to time, while the vertical axis corresponds to frequency. Although the Morlet wavelet transform can have good local characteristics in the time domain frequency domain [26], it may be more accurate to use vibration data to diagnose mechanical faults, while the accuracy of electrical fault diagnosis obtained by current signals may be higher [27]. Due to the process of motor failure, different fault types will obtain one-dimensional information of different order harmonics. In order to observe the amplitude change of the A-phase current, take the logarithm of the amplitude as the ordinate, as shown in Figure 9, when different types of faults occur in the motor, the A-phase current of the motor has different harmonic components, and there are significant variations in harmonic amplitudes.

B. t-SNE VISUALIZATION AND ANALYSIS

To explore and evaluate the ability of wavelet time-frequency images of motor vibration signals and their three-phase current spectra in solving fault classification problems and the possibility of complementary diagnosis. In this paper, t-SNE [28] is introduced to visualize the time-frequency map, a-phase current spectrum, b-phase current spectrum and c-phase current spectrum, respectively. t-SNE visualization can be used to check for the presence of clusters in the data and to see if there is some kind of order or pattern in the data set. And t-SNE is an unsupervised learning algorithm which does not use any labeled data in its work.

Figure 10 shows the t-SNE visualization results of the three-phase current spectrum of the motor, and each point in Figure 10 represents a sample motor operating state. The dots of different colors represent different data labels. In the a-phase and c-phase current spectrum t-SNE visualization images, six clusters can be clearly distinguished, corresponding to SP, SC, RI, BF, NM and BW. In the b-phase current spectrum t-SNE visualization image, only 5 clusters can be clearly distinguished. Among them, RM, BW and SC faults correspond to dark blue, red and purple, respectively, and the dark blue and purple colors almost overlap each other in Figure 10(a) and Figure 10(c), and the three colors overlap each other in Figure 10(b). Therefore, using the single-phase current spectrum of the motor alone for motor fault classification may not be able to accurately classify the BW fault
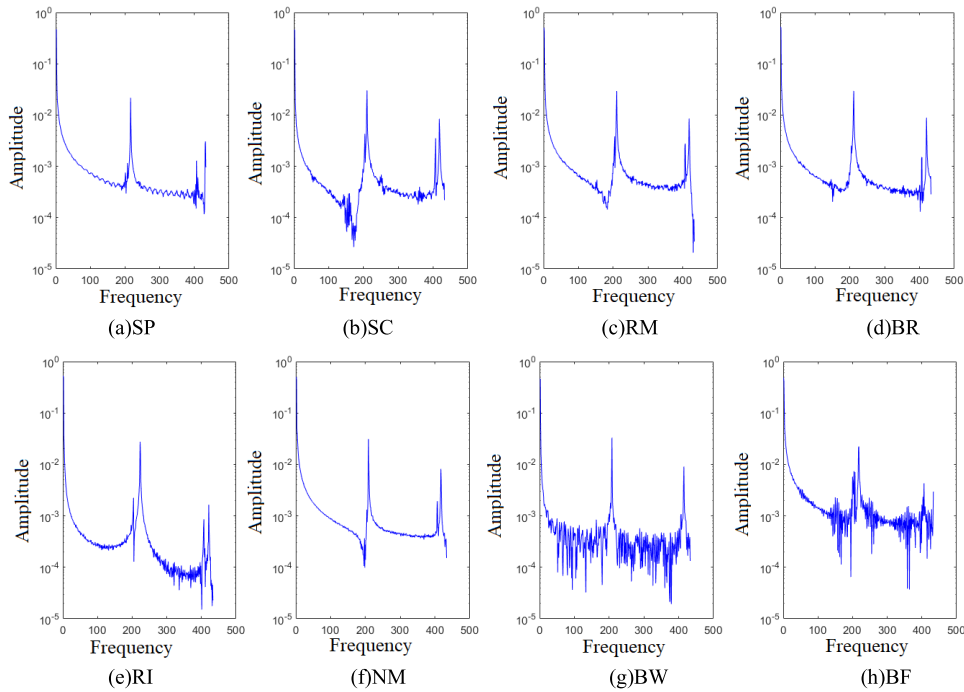
FIGURE 9. A-phase current spectrum in each motor state.

(a)Phase a

(b) Phase b

FIGURE 11. t-SNE implements the visualization of time-frequency graphs.
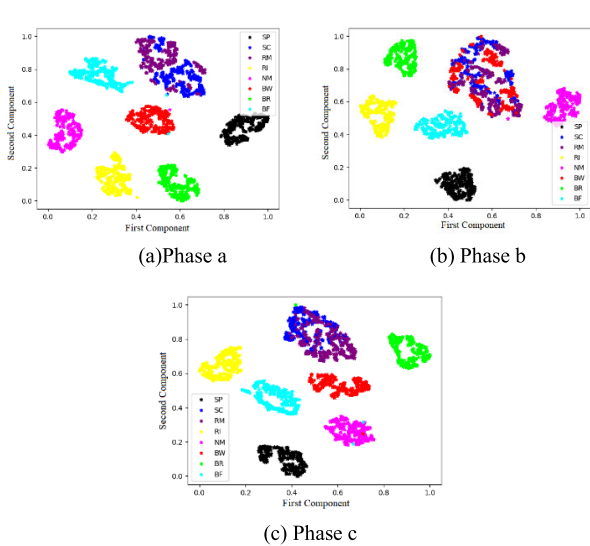

(c) Phase c

FIGURE 10. t-SNE visualizes the three-phase current spectrum of the motor.

of the motor in addition to the RM and SC. And using the three-phase current spectrum for motor fault classification at the same time may only fail to accurately classify RM and SC faults.

Figure 11 shows the results of wavelet time-frequency diagram t-SNE visualization of the motor vibration signal, in which it can be seen that the dark blue, black and green parts corresponding to SC, SP and BR fault overlap each other. However, relative to the three-phase current signal
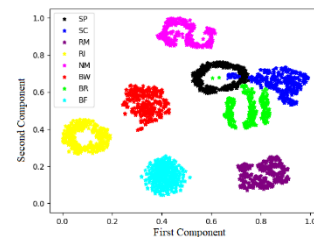
spectrum of the motor, the wavelet time-frequency diagram is able to accurately classify RM, BW and SC.

If the two classification results are fused, the use of wavelet time-frequency diagrams for fault classification can compensate for the ability to classify RM, BW and SC using the current signal spectrum, while the use of three-phase current signal spectrum for fault classification can precisely compensate for the ability to classify SP and BR faults using wavelet time-frequency diagrams.

C. EXPERIMENTAL VERIFICATION AND ANALYSIS

A trail-and-error analysis was carried out to determine the Hybrid CNN-MLPAM model parameters, as showed in Table 4.

Layer Conv1 contained 16 convolution kernels with a size of 5×5 and outputted 16 feature maps with a size of 64×64 (we used zero padding to have the same size of output feature-maps). Layer Max-Poo1 (2×2) outputted 16 pooling maps with a size of 32×32. Layer Conv2 produced 32 feature

TABLE 4. The detailed structure of the designed hybrid CNN-MLPAM model.

| CNN branch			MLP branch	
Input		64×64	Input	433
Conv1	8@5× 5	16@64× 64	Linear1	141 neurons
Max-Pool1	2 × 2	16@32× 32	Linear2	35 neurons
Conv2	16@5× 5	32@32× 32	Linear3	8 neurons
Max-Pool2	2 × 2	32@16× 16	Concatenation	
Conv3	32@3×3	64@16× 16	Linear4	8 neurons
Max-Pool3	2 × 2	64@8× 8		
Conv4	64@3×3	64@8× 8		
Max-Pool4	2 × 2	64@4× 4		
Flatten	1024 neurons			
Linear5	256 neurons + dropout			
Linear6	8 neurons			
Add	$\vec{f_2}*\alpha_2$		$\vec{f_1}*\alpha_1$	
Output	8 neurons			
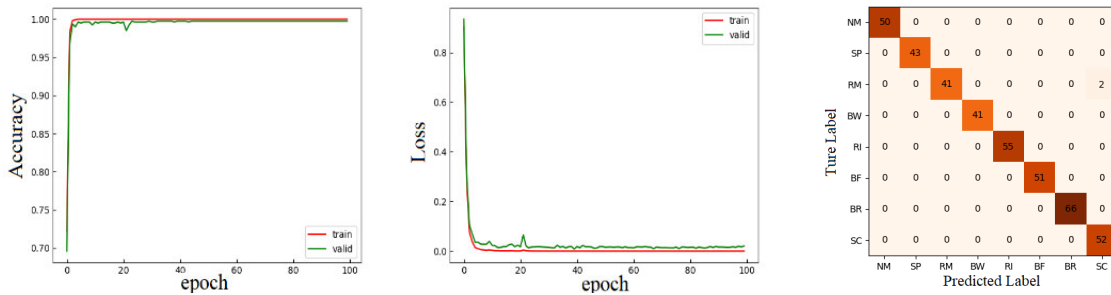
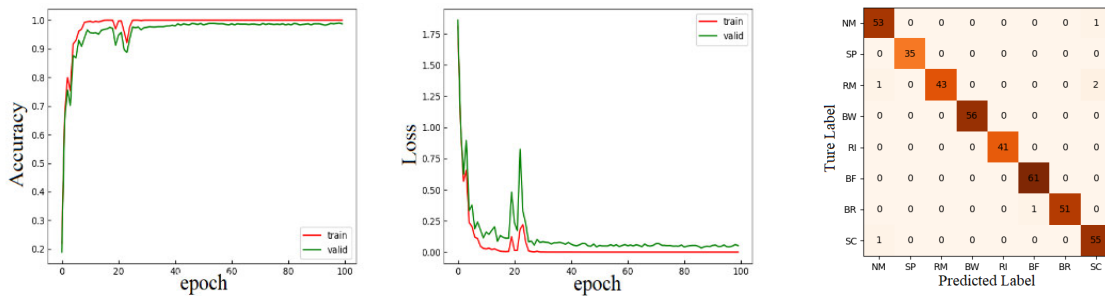**FIGURE 12.** CNN-MLPAM training curve and confusion matrix.

FIGURE 13. CNN-MLP training curve and confusion matrix.

maps with a size of 32×32 and layer Max-Pool2 provided 32 pooling maps with a size of 16×16. After a similar construction of layers Con3, Max-Poo3, Con4, and Max-Poo4, we have 64 pooling maps with a size of 4×4 which than flatten in a layer with 1024 neurons.

An output of CNN from the flatten level is passed to two Dense layers Linear5, Linear6 with the dropout rate 0.2 between them. Another output of MLP form the concatenation layer is passed Linear4. Then the outputs of two models are sent to add layer of weight allocation to an output layer of 8 neurons, which performs data classification.

The operating environment for this article's code is Windows 10 64-bit operating system, 12th Gen Intel®Core™i7-12700H 2.30 GHz, NVIDIA GeForce RTX 3060 Laptop GPU, and 16GB memory. The program running environment is Torch 1.13.1 version. The optimizer used in the model training is the Adam optimizer, which is simple to implement, computationally efficient, requires less
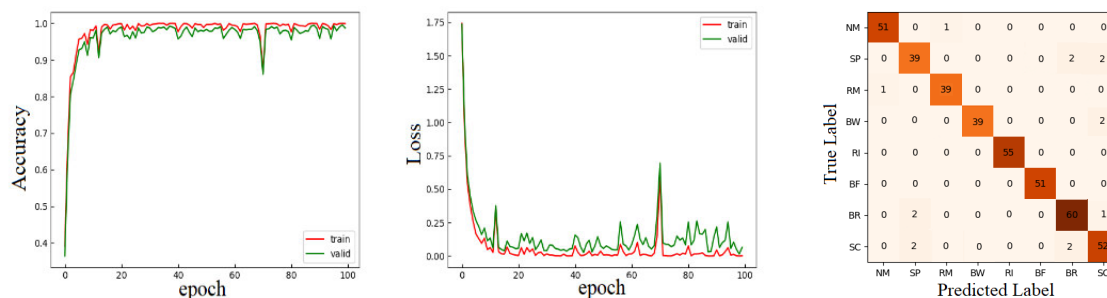
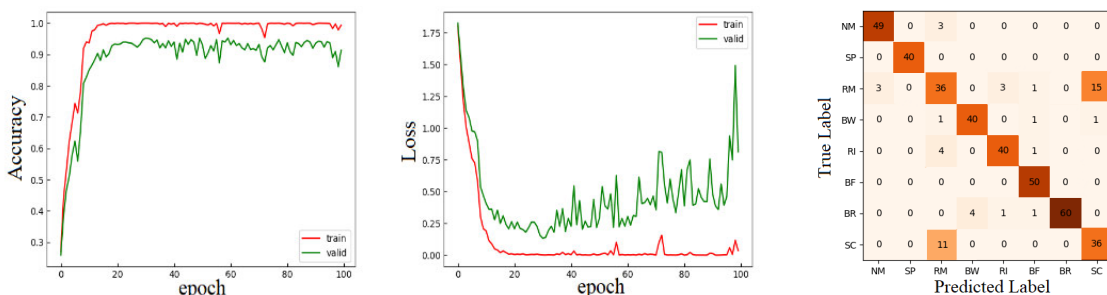**FIGURE 14.** CWT-CNN training curve and confusion matrix.

FIGURE 15. MLP training curve and confusion matrix.

TABLE 5. Classification report for the models.

Models		NM	SP	RM	BW	RI	BF	BR	SC	Accuracy
MLP	precision	0.94	1	0.65	0.91	0.91	0.93	1	0.69	0.88
	recall	0.94	1	0.62	0.98	0.89	1	0.91	0.77	
	F1-score	0.94	1	0.63	0.94	0.90	0.96	0.95	0.73	
CWT-CNN	precision	0.98	0.91	0.97	1	1	1	0.94	0.91	0.96
	recall	0.98	0.91	0.97	1	1	1	0.95	0.93	
	F1-score	0.98	0.91	0.97	1	1	1	0.94	0.92	
CNN-MLP	precision	0.96	1	1	1	1	0.98	1	0.94	0.98
	recall	0.98	1	0.93	1	1	1	0.98	0.98	
	F1-score	0.97	1	0.97	1	1	0.99	0.99	0.96	
CNN-MLPAM	precision	1	1	1	1	1	1	1	0.96	**0.99**
	recall	1	1	1	1	1	1	1	1	
	F1-score	1	1	1	1	1	1	1	0.98	

memory, and can automatically adjust the learning rate, which is initially set to 0.001. All activation functions were the Relu function, the batch size was 64, and the loss function was Categorical Cross entropy function.

The learning curve and confusion matrix of the CNN-MLPAM model are shown in Figure 12. The learning curve shows how the accuracy and loss values of the training and validation datasets change during the training process, and the figure shows that the training accuracy of the validation set is stable at 99.95%. The training of the hybrid CNN-MLPAM model was stopped at the 100th epochs, and the model trained at the 82nd epochs was used as the model with the lowest value of the loss function in the validation set. In addition, the accuracy of the model is tested using the test set. The testing results are shown in the confusion matrix on the right side of Figure 12. From the confusion matrix of the

CNN-MLPAM model, it can be seen that all eight states of the motor can be correctly classified, and the diagnostic accuracy of the CNN-MLPAM model is further improved compared with the hybrid MLP-CNN model.

Similarly, when the attention mechanism module is removed, the output features of FC and CNN are concatenated to obtain the hybrid MLP-CNN model. The learning curve and confusion matrix of the CWT-CNN model, mixed MLP-CNN model, and MLP model based on three-phase current are separately analyzed and shown in Figure 13, 14 and 15. In Figure 14, the training and validation curves of the CWT-CNN model have large fluctuations during the training process. For the CWT-CNN model, there are 15 instances of misclassification. Among them, four SP faults and four SC faults were misclassified, and two BR samples were misclassified. As shown in the confusion matrix
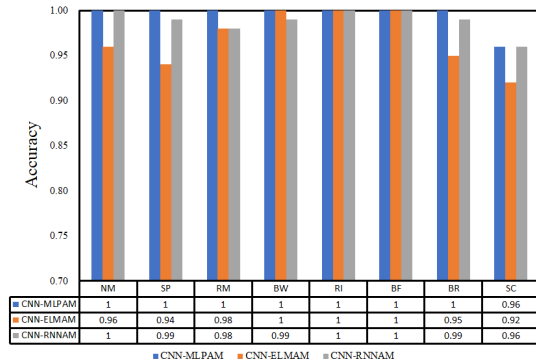
FIGURE 16. The accuracy of different algorithms is compared under different fault types.

TABLE 6. Comparison of the runtime of different methods.

Models	Max-acc(%)	Avg-acc(%)	Training time(s)	Testing time (s per epoch)
CNN-MLPAM	99.35	98.61±0.58	321	0.39
CNN-ELMAM	98.75	97.75±1.08	272	0.22
CNN-RNNAM	99.51	99.14±0.68	474	0.43
CNN-MLP	99.25	97.91±1.21	206	0.12
CWT-CNN	97.25	95.80±1.36	158	0.15
LSTM-BLS[32]	97.51	96.50±1.07	166	0.16
VMD-CWT-CNN[33]	98.25	95.60±2.18	182	0.17
PSO-CNN[34]	98.25	97.20±0.82	291	0.27
IGWO-DBN[35]	98.25	95.60±2.14	150	0.15
MLP	90.05	86.66±3.78	11	0.01

in Figure 15, the MLP model can accurately identify BR and SP faults. However, due to the harmonic components similar to SC that can be generated by RM faults [29], [30], the diagnostic accuracy of the MLP model for these two faults is lower. On the other hand, the CWT-CNN model can better identify SC and RM faults, so mixing these two diagnostic models can complement each other successfully, and significantly reduces the produced errors.

The diagnostic model in this paper is a multiclassification model. Thus, the diagnostic performance of the proposed method will be further evaluated in 4 aspects: accuracy, precision, recall, and F1 score [31]. These 4 metrics are calculated as in

$$Accuracy = \frac{TP + TN}{TP + TN + FN + FP} \tag{7}$$

$$Recall = \frac{TP}{TP + TN} \tag{8}$$

$$Precision = \frac{TP}{TP + FP} \tag{9}$$

$$F1 = \frac{2 \times Precision \times Recall}{Precision + Recall} \tag{10}$$

where TP, TN, FN, and FP denote the number of true positive samples, true negative samples, false negative samples, and false positive samples, respectively. Obviously, the higher accuracy rate represents the better diagnostic performance of the model.
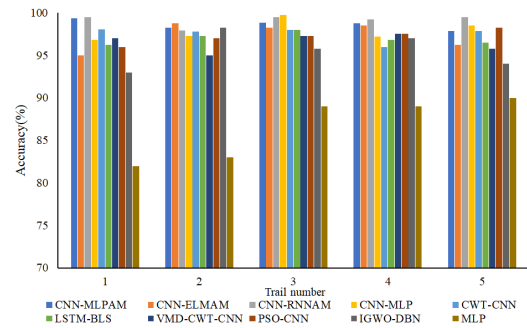

FIGURE 17. The classification accuracy of each trail.

The accuracy, recall, precision, and F1 score for each motor fault category and each model. In the table, it can be seen that for the CWT -CNN model, the accuracies of stator single-phase disconnection, rotor broken bar, and turn-to-turn short circuit diagnosis are 0.91, 0.94, and 0.91, respectively. For the MLP model, the accuracies of stator single-phase disconnection and rotor broken bar fault diagnosis are 1, and the accuracies of rotor eccentricity fault and turn-to-turn short circuit diagnosis are 0.65 and 0.65, respectively. The combination of motor vibration signal and three-phase current signal for motor fault diagnosis enables the complementary electrical and mechanical fault diagnosis of the motor, thus enabling CNN-MLP to complementary diagnosis and further improve the diagnosis accuracy. Meanwhile, in Section III-B, the three-phase current spectrum and wavelet time-frequency image classification analysis of the motor using t-SNE predicts that it may be difficult to identify the rotor eccentricity and turn-to-turn short circuit faults of the motor.

D. COMPARISON AND ANALYSIS WITH OTHER METHODS
To evaluate the performance of the proposed model, several deep learning models were compared on the same data and using the same network structure parameters as in this paper. The commonly used three deep learning models for extracting numerical features of the three-phase current in motors were the recurrent neural network (RNN), extreme learning machine (ELM), as shown in Figure.16, the CNN-ELMAM and CNN-RNNAM diagnostic models achieved accuracies of 92% and 96% for inter-turn short circuit diagnosis, respectively, in the test set. Compared to the other algorithms, the CNN-MLPAM had higher diagnostic accuracy for motor inter-turn short circuits, rotor bending, rotor eccentricity, and stator single-phase open circuit faults. Among them, the CNN-RNNAM diagnostic model also showed high diagnostic accuracy in the test set, with an average diagnostic accuracy of 98.87% for the eight motor faults.

To further prove the validity of the CNN-MLPAM algorithm, a comparison experiment of the proposed method with recent related literature is carried out. The overall classification accuracy was chosen as the evaluation metric,
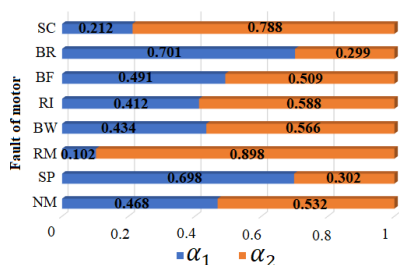
FIGURE 18. Attention weight distribution.

including maximum accuracy, average accuracy, training time, and diagnostic time for a single instance from the test set. The diagnostic results from the test set are shown in Figure.17 and Table 6.

From Figure 17 and Table 6, it can be observed that compared to other diagnostic models, CNN-MLPAM exhibits stronger stability. The diagnostic accuracies of CNN-MLPAM on the test set for five training runs are 99.75%, 98.25%, 98.85%, 98.75%, and 97.85%, with an average diagnostic accuracy of 98.61% and a standard deviation of 0.58%. CNN-RNNAM can achieve high diagnostic accuracies, but CNN-RNNAM requires longer training time and consumes significant computational resources. From Table 6, it can be observed that introducing the attention mechanism module can improve the diagnostic accuracy of the model and enhance the stability of CNN-MLP, but it will also increase the model's training time and the diagnosis time per test sample.

The methods mentioned in [32], [33], [34], and [35] were applied to motor fault diagnosis, achieving average accuracies of 96.5%, 95.6%, 97.2%, and 95.6%, respectively, with standard deviations of 1.07%, 2.18%, 0.82%, and 2.14%. Among them, VMD-CWT-CNN and IGWO-DBN have poorer stability. VMD-CWT-CNN utilizes the IMF components obtained through VMD decomposition, concatenates the reconstructed data of IMF, and performs overlap sampling to expand the sample dataset, making it more suitable for small-sample fault diagnosis. The model parameters of IGWO-DBN are optimized by GWO, and if the optimization algorithm fails to converge effectively or falls into a local optimum, the stability of the model may be affected. PSO-CNN achieves good accuracy by optimizing the number of convolutional kernels in the CNN convolutional layer and the learning rate using PSO, but it also significantly increases computational cost. In summary, solely relying on vibration signals for motor fault diagnosis may restrict the diagnostic performance of the model and may not be sufficient to further improve the diagnostic accuracy.

E. DISCUSSION ABOUT ATTENTION DISTRIBUTION WEIGHTS

To further analyze the role of the attention mechanism on the CNN-MLPAM model generation, thus the weights α_1 and α_2 2 are analyzed. The distribution of attention weights

for the fusion of motor vibration and current data is shown in Figure.18. For the same fault, the proportions of the two measurement methods are not the same. In the BR and SP faults, the motor current data occupy a larger weight, while in the RM, BF, and SC faults, the motor vibration data occupy a larger weight. The motor current signal may be relatively sensitive to electrical faults compared to the motor vibration data [10]. Therefore, different measurement methods have different sensitivities for different faults. The attention mechanism can be used to assign more weights to the measurement methods with higher diagnostic accuracy, thus further improving the diagnostic accuracy of the model. At the same time, the process of assigning weights in the attention mechanism model can also verify that different measurement methods have different sensitivities to different fault types. Embedding the attention mechanism into the CNN-MLP model makes the diagnostic accuracy of the CNN-MLPAM model up to 99%.

IV. CONCLUSION

This article proposes a motor fault diagnosis method based on an attention mechanism CNN-MLP hybrid model. The model simultaneously processes different types of data, with three MLP branches processing the frequency spectrum of the motor's three-phase current signals, and CNN processing CWT images. It uses attention distribution to combine the output result vectors of the MLP and CNN modules, constructing attention distribution between different data information to focus on fault-sensitive data during the fault diagnosis process and achieve a complementary diagnosis, thereby improving the accuracy of motor fault diagnosis. This method was validated using relevant data from a motor fault experimental platform, achieving a fault diagnosis accuracy rate of over 99% in the experimental case. The experimental results show that CNN-MLPAM is superior to other models, such as CNN, MLP, and CNN-MLP, with a diagnosis accuracy rate of 99% for motor faults. Compared with CNN-RNNAM and CNN-ELMAM, CNN-RNNAM has higher cost-effectiveness in diagnosing faults while considering time cost and high diagnosis accuracy. In addition, with the rapid development of fault diagnosis technology, this method can be applied to future industrial scenarios. In the future, it will further analyze the mechanism of inter-turn short-circuit and rotor eccentricity faults, and introduce the electromagnetic or acoustic signals of motors to realize the multi-sensor information-driven motor fault diagnosis.

REFERENCES

[1] Y. Liu and A. M. Bazzi, "A review and comparison of fault detection and diagnosis methods for squirrel-cage induction motors: State of the art," *ISA Trans.*, vol. 70, pp. 400–409, Sep. 2017.

[2] A. Kumar, C. P. Gandhi, Y. Zhou, H. Tang, and J. Xiang, "Fault diagnosis of rolling element bearing based on symmetric cross entropy of neutrosophic sets," *Measurement*, vol. 152, Feb. 2020, Art. no. 107318.

[3] A. Kumar, Y. Zhou, and J. Xiang, "Optimization of VMD using kernel-based mutual information for the extraction of weak features to detect bearing defects," *Measurement*, vol. 168, Jan. 2021, Art. no. 108402.

[4] B. Bessam, A. Menacer, M. Boumehraz, and H. Cherif, "Detection of broken rotor bar faults in induction motor at low load using neural network," *ISA Trans.*, vol. 64, pp. 241–246, Sep. 2016.

[5] J. C. Quiroz, N. Mariun, M. R. Mehrjou, M. Izadi, N. Misron, and M. A. M. Radzi, "Fault detection of broken rotor bar in LS-PMSM using random forests," *Measurement*, vol. 116, pp. 273–280, Feb. 2018.

[6] A. Choudhary, D. Goyal, and S. S. Letha, "Infrared thermography-based fault diagnosis of induction motor bearings using machine learning," *IEEE Sensors J.*, vol. 21, no. 2, pp. 1727–1734, Jan. 2021.

[7] D. M. Sonje, P. Kundu, and A. Chowdhury, "A novel approach for sensitive inter-turn fault detection in induction motor under various operating conditions," *Arabian J. Sci. Eng.*, vol. 44, no. 8, pp. 6887–6900, Mar. 2019.

[8] A. L. O. Vitor, A. Goedtel, S. Barbon, G. H. Bazan, M. F. Castoldi, and W. A. Souza, "Induction motor short circuit diagnosis and interpretation under voltage unbalance and load variation conditions," *Exp. Syst. Appl.*, vol. 224, Aug. 2023, Art. no. 119998.

[9] M. Irhoumah, R. Pusca, E. Lefèvre, D. Mercier, and R. Romary, "Stray flux multi-sensor for stator fault detection in synchronous machines," *Electronics*, vol. 10, p. 2313, Sep. 2021.

[10] Z. Long, X. Zhang, L. Zhang, G. Qin, S. Huang, D. Song, H. Shao, and G. Wu, "Motor fault diagnosis using attention mechanism and improved AdaBoost driven by multi-sensor information," *Measurement*, vol. 170, Jan. 2021, Art. no. 108718.

[11] A. Choudhary, R. K. Mishra, S. Fatima, and B. K. Panigrahi, "Multi-input CNN based vibro-acoustic fusion for accurate fault diagnosis of induction motor," *Eng. Appl. Artif. Intell.*, vol. 120, Apr. 2023, Art. no. 105872.

[12] H. Cherif, A. Benakcha, I. Laib, S. E. Chehaidia, A. Menacer, B. Soudan, and A. G. Olabi, "Early detection and localization of stator inter-turn faults based on discrete wavelet energy ratio and neural networks in induction motor," *Energy*, vol. 212, Dec. 2020, Art. no. 118684.

[13] Y. Xu, X. Yan, B. Sun, and Z. Liu, "Global contextual residual convolutional neural networks for motor fault diagnosis under variable-speed conditions," *Rel. Eng. Syst. Saf.*, vol. 225, Sep. 2022, Art. no. 108618.

[14] P. Fu, J. Wang, X. Zhang, L. Zhang, and R. X. Gao, "Dynamic routing-based multimodal neural network for multi-sensory fault diagnosis of induction motor," *J. Manuf. Syst.*, vol. 55, pp. 264–272, Apr. 2020.

[15] A. Glowacz, "Fault diagnosis of single-phase induction motor based on acoustic signals," *Mech. Syst. Signal Process.*, vol. 117, pp. 65–80, Feb. 2019.

[16] D. Xiao, C. Qin, H. Yu, Y. Huang, and C. Liu, "Unsupervised deep representation learning for motor fault diagnosis by mutual information maximization," *J. Intell. Manuf.*, vol. 32, no. 2, pp. 377–391, Feb. 2021.

[17] A. Mohammed and S. Djurovic, "FBG thermal sensing ring scheme for stator winding condition monitoring in PMSMs," *IEEE Trans. Transport. Electrific.*, vol. 5, no. 4, pp. 1370–1382, Dec. 2019.

[18] Z. Ullah, S.-T. Lee, and J. Hur, "A torque angle-based fault detection and identification technique for IPMSM," *IEEE Trans. Ind. Appl.*, vol. 56, no. 1, pp. 170–182, Jan. 2020.

[19] B. Ren, M. Yang, N. Chai, Y. Li, and D. Xu, "Fault diagnosis of motor bearing based on speed signal kurtosis spectrum analysis," in *Proc. 22nd Int. Conf. Electr. Mach. Syst. (ICEMS)*, Harbin, China, Aug. 2019, pp. 1–6.

[20] Q. Hu, X.-S. Si, Q.-H. Zhang, and A.-S. Qin, "A rotating machinery fault diagnosis method based on multi-scale dimensionless indicators and random forests," *Mech. Syst. Signal Process.*, vol. 139, May 2020, Art. no. 106609.

[21] M. Singh and A. G. Shaik, "Incipient fault detection in stator windings of an induction motor using Stockwell transform and SVM," *IEEE Trans. Instrum. Meas.*, vol. 69, no. 12, pp. 9496–9504, Dec. 2020.

[22] O. Yaman, "An automated faults classification method based on binary pattern and neighborhood component analysis using induction motor," *Measurement*, vol. 168, Jan. 2021, Art. no. 108323.

[23] S. R. Saufi, Z. A. B. Ahmad, M. S. Leong, and M. H. Lim, "Challenges and opportunities of deep learning models for machinery fault detection and diagnosis: A review," *IEEE Access*, vol. 7, pp. 122644–122662, 2019.

[24] Y. Li, Y. Wang, Y. Zhang, and J. Zhang, "Diagnosis of inter-turn short circuit of permanent magnet synchronous motor based on deep learning and small fault samples," *Neurocomputing*, vol. 442, pp. 348–358, Jun. 2021.

[25] R. Liu, F. Wang, B. Yang, and S. J. Qin, "Multiscale kernel based residual convolutional neural network for motor fault diagnosis under nonstationary conditions," *IEEE Trans. Ind. Informat.*, vol. 16, no. 6, pp. 3797–3806, Jun. 2020.

[26] L. P. A. Arts and E. L. van den Broek, "The fast continuous wavelet transformation (fCWT) for real-time, high-quality, noise-resistant time-frequency analysis," *Nature Comput. Sci.*, vol. 2, no. 1, pp. 47–58, Jan. 2022.

[27] Z. Liu and L. Zhang, "A review of failure modes, condition monitoring and fault diagnosis methods for large-scale wind turbine bearings," *Measurement*, vol. 149, Jan. 2020, Art. no. 107002.

[28] L. van der Maaten and G. Hinton, "Visualizing data using t-SNE," *J. Mach. Learn. Res.*, vol. 9, pp. 2579–2605, Nov. 2008.

[29] A. Sapena-Bano, J. Martinez-Roman, R. Puche-Panadero, M. Pineda-Sanchez, J. Perez-Cruz, and M. Riera-Guasp, "Induction machine model with space harmonics for the diagnosis of rotor eccentricity, based on the convolution theorem," *Int. J. Electr. Power Energy Syst.*, vol. 117, May 2020, Art. no. 105625.

[30] A. Mojtaba, A. Salman, O. Ashknaz, E. Mohammad, and M. Richard, "Eccentricity fault detection in brushless doubly fed induction machines," *IET Electr. Power Appl.*, vol. 15, pp. 916–930, Mar. 2021.

[31] L. Jia, T. W. S. Chow, and Y. Yuan, "GTFE-Net: A gramian time frequency enhancement CNN for bearing fault diagnosis," *Eng. Appl. Artif. Intell.*, vol. 119, Mar. 2023, Art. no. 105794.

[32] S. Zhao, C. Zhang, and Y. Wang, "Lithium-ion battery capacity and remaining useful life prediction using board learning system and long short-term memory neural network," *J. Energy Storage*, vol. 52, Aug. 2022, Art. no. 104901.

[33] J. Gu, Y. Peng, H. Lu, X. Chang, and G. Chen, "A novel fault diagnosis method of rotating machinery via VMD, CWT and improved CNN," *Measurement*, vol. 200, Aug. 2022, Art. no. 111635.

[34] W. Fuan, J. Hongkai, S. Haidong, D. Wenjing, and W. Shuaipeng, "An adaptive deep convolutional neural network for rolling bearing fault diagnosis," *Meas. Sci. Technol.*, vol. 28, no. 9, 2017, Art. no. 095005.

[35] Z. Jin, D. He, and Z. Wei, "Intelligent fault diagnosis of train axle box bearing based on parameter optimization VMD and improved DBN," *Eng. Appl. Artif. Intell.*, vol. 110, Apr. 2022, Art. no. 104713.

YI ZHOU received the B.S. degree from the School of Mechanical and Engineering, Wuhan University of Engineering Science, Wuhan, China, in 2021. He is currently pursuing the master's degree in marine engineering with the Wuhan University of Technology, Wuhan. His research interests include data-driven fault detection and diagnosis, fault prediction, and digital twin technology.

QIANMING SHANG received the B.S. and M.S. degrees in marine engineering from the Wuhan University of Technology, Wuhan, China, in 1998 and 2001, where he is currently pursuing the Ph.D. degree in marine engineering. He is currently an Associate Professor with the Wuhan University of Technology. His research interests include marine simulation and system control, digital twin technology, intelligent ship machine learning, and deep learning methods.

CONG GUAN (Member, IEEE) received the B.S., M.S., and Ph.D. degrees in marine engineering from the Wuhan University of Technology, Wuhan, China, in 2010, 2012, and 2015, respectively. He is currently an Associate Professor at the Wuhan University of Technology. His research interests include simulation and control technology and modeling of ship power systems.

• • •